Journal of
Nanophotonics

Nanophotonics.SPIEDigitalLibrary.org

Achieving angle-insensitive spectrum filter with the slit nanoresonator array structure

Jing Zhou
L. Jay Guo

Achieving angle-insensitive spectrum filter with the slit nanoresonator array structure

Jing Zhou and L. Jay Guo*
University of Michigan, Department of Electrical Engineering and Computer Science,
Ann Arbor, Michigan 48109, United States

Abstract. The spectrum filtering behavior of the slit nanoresonator array structure is based on the coupling between the slit resonance and the Wood's anomaly of grating array, and therefore has angle dependence, which is not desirable for some applications. To achieve an angle-insensitive spectrum filter, such a coupling should be disrupted. We show that reducing the period of the slit array helps decouple these two resonances. Additionally, by enhancing the light confinement inside the slits through either shrinking the slit width or filling the slits with a high-index medium, a narrow transmission peak is maintained at a small period so that an angle-insensitive spectrum filter is achieved. © *2015 Society of Photo-Optical Instrumentation Engineers (SPIE)* [DOI: 10.1117/1.JNP.9.093795]

Keywords: spectrum filers; subwavelength structures; resonators; gratings.

Paper 14089SS received Aug. 23, 2014; accepted for publication Nov. 25, 2014; published online Dec. 22, 2014.

1 Introduction

Subwavelength metallic grating-based structures have been exploited for structural colors.[1–4] Metallic nanoslits have been proposed as angle-insensitive color filters based on the localized Fabry-Perot resonance of transverse magnetic (TM) light in each slit.[2,3] By forming a dense array, the slit nanoresonators could provide high efficiency and find practical applications in high-resolution visual displays, miniature hyperspectral imaging, and high-sensitivity sensors.[5–7] Especially, they could be a potential replacement of the colorant pigments widely used in LCD displays and colored imagers.[2,8] However, the periodic arrangement inherently produces grating resonances (i.e., diffractions or Wood's anomaly), which could couple with the slit resonance and make the spectrum filtering behavior angle dependent.[9–13] This characteristic is undesirable for display and imaging applications. We propose a solution to address this issue: by reducing the grating period, the grating resonance is decoupled from the slit resonance so that the transmission becomes much less angle dependent. By enhancing the light confinement inside the slits through either shrinking the slit width or filling the slits with a high-index medium, a narrow transmission peak is maintained at a small period and thus an angle-insensitive spectrum filter is obtained.

2 Analytical Model of the Slit Array

Consider a typical perforating metal slit array supported by a dielectric substrate as sketched in Fig. 1. The slit width, the slit height, and the period are denoted as a, h, and d, respectively. The whole space is then divided into three regions: air above the metal layer (I), the metal layer with perforating slits (II), and the dielectric substrate (III).

The response of this structure to a TM light is analytically derived.[3] First, the light field (represented by the TM field H_z) in regions I and III is expressed by Rayleigh's expansion as following:

---

*Address all correspondence to: L. Jay Guo, E-mail: guo@umich.edu

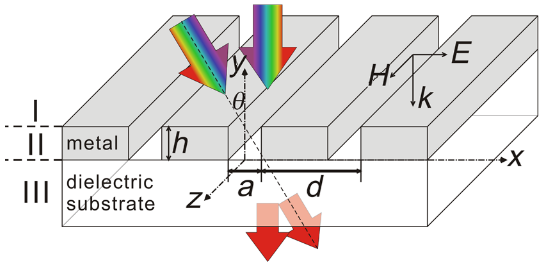

Fig. 1 Sketch of a metallic nanoslit array.

$$H_z^{\mathrm{I}} = \sum_{m=-\infty}^{+\infty} \{ r_m \exp[i\chi_m^{\mathrm{I}}(y-h)] + \delta_{m,0} \exp[-i\chi_0 y] \} \exp(i\tilde{\alpha}_0 x) \exp(i\alpha_m x), \tag{1}$$

$$H_z^{\mathrm{III}} = \sum_{m=-\infty}^{+\infty} t_m \exp(-i\chi_m^{\mathrm{III}} y) \exp(i\tilde{\alpha}_0 x) \exp(i\alpha_m x). \tag{2}$$

The field in region I is a superposition of incident and reflection light. The field in region III represents transmission. r_m and t_m are the m'th order reflection and transmission coefficients, respectively. $\delta_{m,0}$ equals 1 at $m = 0$ and equals 0 for other cases. $\tilde{\alpha}_0 = k_0 \sin\theta$ denotes the x component of the wave vector; and $\alpha_m = 2m\pi/d$ represents the m'th order extra momentum provided by the grating. $\chi_m^{\mathrm{I}} = \sqrt{k_0^2 - (\tilde{\alpha}_0 + \alpha_m)^2}$ and $\chi_m^{\mathrm{III}} = \sqrt{\varepsilon_{\mathrm{d}} k_0^2 - (\tilde{\alpha}_0 + \alpha_m)^2}$ represent the y-directional momentum of the photons in regions I and III, respectively. ε_{d} is the dielectric constant of the substrate. In region II, if the metal is assumed to be perfectly conductive, the field inside the metal is zero and that inside each slit can be described as a superposition of the waveguide modes. When the wavelength is much larger than the slit width, only the fundamental mode is taken into account. With these two approximations, the field in region II writes

$$H_z^{\mathrm{II}} = \begin{cases} [a^+ \exp(i\beta y) + a^- \exp(-i\beta y)] \exp(i\tilde{\alpha}_0 x), & \text{slit area} \\ 0, & \text{metal area} \end{cases}. \tag{3}$$

The light field inside each slit is regarded as a superposition of two fundamental slit waveguide modes, i.e., $a^+ \exp(i\beta y)$ and $a^- \exp(-i\beta y)$, propagating in the positive and the negative y-directions, respectively. β is the propagation constant of the slit waveguide mode. It is equal to k_0 when the slits are empty, and changes into $\sqrt{\varepsilon_{\mathrm{s}}} k_0$ when the slits are filled by a material with a dielectric constant of ε_{s}. At the I/II and II/III interfaces, the continuity of the tangential components of the field implies that E_x and H_z are continuous within the slit interval $(-a/2 + n'd \le x \le a/2 + n'd,\ n'$ is an integer) and $E_x = 0$ within the metal interval $[(-d/2 + n'd \le x < -a/2 + n'd) \cup (d/2 + n'd < x \le a/2 + n'd)]$. The boundary conditions together with the narrow-slit approximation determine the coefficients a^+, a^-, r_m, and t_m:

$$r_a = \frac{a^+}{a^-} = \frac{\sum_{m=-\infty}^{+\infty} \frac{a}{d} \operatorname{sinc}\left(\alpha_m \frac{a}{2}\right) \left(\frac{\varepsilon_d}{-i\chi_m^{\mathrm{III}}}\right) \left(\frac{i\beta}{\varepsilon_{\mathrm{s}}}\right) + 1}{\sum_{m=-\infty}^{+\infty} \frac{a}{d} \operatorname{sinc}\left(\alpha_m \frac{a}{2}\right) \left(\frac{\varepsilon_d}{-i\chi_m^{\mathrm{III}}}\right) \left(\frac{i\beta}{\varepsilon_{\mathrm{s}}}\right) - 1}, \tag{4}$$

$$a^- = \frac{2 \exp(-i\chi_0^{\mathrm{I}} h)}{\exp(-i\beta h) \left[\sum_{m=-\infty}^{+\infty} \frac{a}{d} \operatorname{sinc}\left(\alpha_m \frac{a}{2}\right) \frac{\beta}{\varepsilon_{\mathrm{s}} \chi_m^{\mathrm{I}}} + 1\right] - r_a \exp(i\beta h) \left[\sum_{m=-\infty}^{+\infty} \frac{a}{d} \operatorname{sinc}\left(\alpha_m \frac{a}{2}\right) \frac{\beta}{\varepsilon_{\mathrm{s}} \chi_m^{\mathrm{I}}} - 1\right]}, \tag{5}$$

$$r_m = \frac{a}{d} \operatorname{sinc}\left(\alpha_m \frac{a}{2}\right) \frac{\beta}{\varepsilon_{\mathrm{s}} \chi_m^{\mathrm{I}}} [a^+ \exp(i\beta h) - a^- \exp(-i\beta h)] + \delta_{m,0} \exp(-i\chi_m^{\mathrm{I}} h), \tag{6}$$

$$t_m = \frac{a}{d} \operatorname{sinc}\left(\alpha_m \frac{a}{2}\right) \left(\frac{\varepsilon_d}{-i\chi_m^{\mathrm{III}}}\right) \left(\frac{i\beta}{\varepsilon_{\mathrm{s}}}\right) (a^+ - a^-). \tag{7}$$

Due to the subwavelength scale, the zeroth-order transmitted light is of most concern. By working out the transmitted fields with the coefficients in Eqs. (4)–(7), the zeroth-order transmission is derived as

$$T_0 = |t_0|^2 \frac{\sqrt{\varepsilon_\mathrm{d} k_0^2 - \tilde{\alpha}_0^2}/\varepsilon_\mathrm{d}}{\sqrt{k_0^2 - \tilde{\alpha}_0^2}}, \tag{8}$$

where t_0 is the zeroth-order transmission coefficient that can be derived from Eq. (7). For the metal slit array with $a = 110$ nm and $h = 170$ nm on a fused silica substrate ($\varepsilon_\mathrm{d} = 2.10$), the zeroth-order transmission at normal incidence is plotted versus wavelength and period as a two-dimensional (2-D) contour [Fig. 2(a)].

The red wedge zone corresponds to the resonant transmission peak, which is used for spectrum filtering. The oblique dark lines (marked as white dashed lines) represent the different diffraction orders of Wood's anomaly.[9] They are divided into two sets: $N' = 1$ and $N' = 2$ represent the first- and the second-order grating resonances at the grating/substrate interface, while $N = 1$ and $N = 2$ represent the diffractions at the grating/air interface. The transmission peak

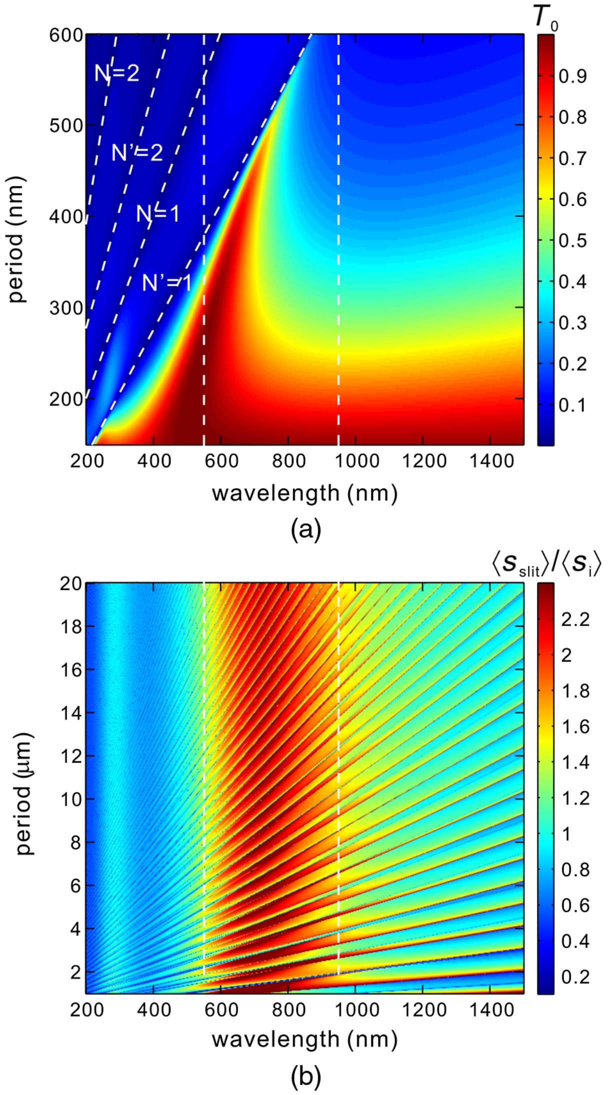

Fig. 2 Zeroth-order normal incidence transmission (T_0) (a) and slit power enhancement factor ($\langle S_\mathrm{slit}\rangle/\langle S_\mathrm{i}\rangle$) (b) versus wavelength and period. The slit width is 110 nm and the height is 170 nm. The inclining dashed lines mark out the Wood's anomalies. The area between the two vertical dashed lines marks out the slit resonance.

(red wedge zone) is a result of the coupling between the Wood's anomaly and the slit resonance. The slit resonance is caused by the Fabry-Perot effect of the waveguide modes in each slit. The red shift of the transmission peak with increasing period just follows the lower branch of the anti-crossing. With increasing period, the ratio of the slit area to period decreases and thus the transmission decreases so that the coupling between the slit resonance and higher-order Wood's anomalies becomes too weak to be shown in Fig. 2(a). In order to more explicitly reveal the slit resonance as well as its coupling with higher-order Wood's anomalies, the slit power enhancement factor,[3] which is the ratio of the power flow inside each slit ($\langle S_{\mathrm{slit}}\rangle$) to that of the incident light ($\langle S_{\mathrm{i}}\rangle$), is plotted versus wavelength and period in Fig. 2(b). The expression is

$$\frac{\langle \mathrm{S}_{\mathrm{slit}}\rangle}{\langle \mathrm{S}_{\mathrm{i}}\rangle} = \frac{1}{\sqrt{\varepsilon_s}}(|a^-|^2 - |a^+|^2). \tag{9}$$

This quantity represents how much power flows through the slits. Since the light power inside the slits is directly influenced by slit resonances and it encompasses all diffraction orders, the slit power enhancement factor is more sensitive to the slit dimension itself than to the grating period. As shown in Fig. 2(b), the slit resonance is intrinsically independent of the period due to the localized nature. This is indicated in Fig. 2(b) as well as in Fig. 2(a) by the two vertical dashed lines. Since the transmission peak, which would serve to filter the spectrum, is a hybrid of the slit resonance and the Wood's anomaly, it inherits period as well as angle dependence from the Wood's anomaly. In this theoretical model, the metal is approximated to be a perfect conductor. However, the analysis of the coupling between the slit resonance and the Wood's anomaly can be applied to real metal cases as well (see Sec. 6). The only difference is that the Wood's anomaly becomes surface plasmon polariton (SPP)-mediated destructive interference[14] and the slit waveguide mode becomes a metal-insulator-metal (MIM) SPP waveguide mode.

3 Reducing the Angle-Dependence by Decreasing the Period

One solution to achieve an angle-insensitive spectrum filter is to decouple the Wood's anomaly from the slit resonance. This can be done by reducing the grating period so that the Wood's anomaly gradually moves to shorter wavelengths (Fig. 2). Take the metal slit array with $a = 110$ nm and $h = 170$ nm on a fused silica substrate as an example. The zeroth-order transmission is plotted as a function of wavelength and incident angle at the periods of 300 and 400 nm in Figs. 3(a) and 3(b). As shown, by reducing the period from 400 to 300 nm, the angle-insensitive range of the transmission peak (marked by the thicker dashed line) is increased from 0 deg to 4 deg to 0 deg to 8 deg.

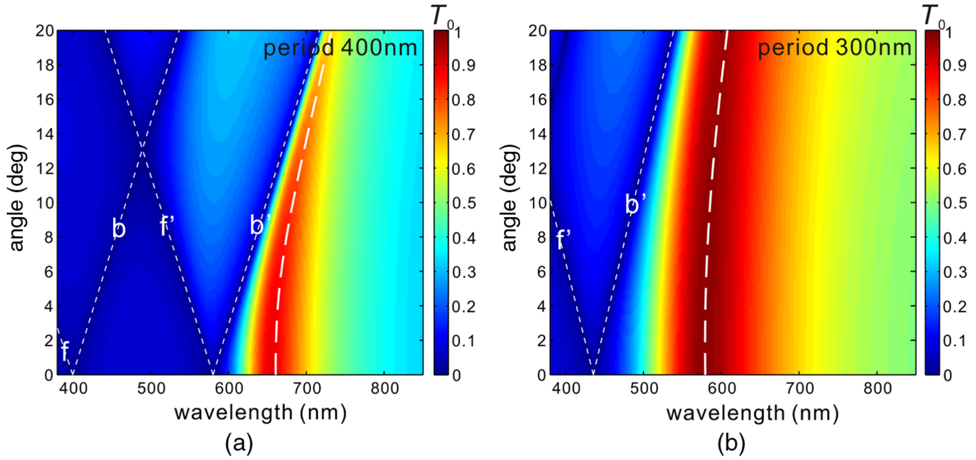

(a)

(b)

Fig. 3 Angle-dependent transmission spectra at the periods of 400 nm (a) and 300 nm (b). The slit width is 110 nm and the height is 170 nm. The thin dashed lines mark out the Wood's anomalies. The thick dashed line marks out the transmission peak.

In the 2-D contour of angle-dependent transmission spectra, each grating resonance splits into two branches due to the phase matching requirement. One shifts to shorter wavelengths, representing the forward diffraction whose x-component wavevector (k_x) has the same sign as that of the incident light. The other shifts to longer wavelengths, representing the backward diffraction whose k_x has the opposite sign to that of the incident light. f and f' denote the forward diffractions at the grating/air interface and at the grating/substrate interface, respectively; b and b' denote the backward diffractions. At the period of 400 nm, the origin of the f' and the b' branch is close to the slit resonance so that the b' branch starts to overlap with the slit resonance at ∼4 deg and form a coupled grating/slit resonance, which is angle dependent. At the period of 300 nm, the grating resonances move to shorter wavelengths [the f and the b branches are even shifted to UV range so that they become invisible in Fig. 3(b)]. Thus, the b' branch does not couple with the slit resonance until 8 deg. To achieve an angle insensitive range up to 60 deg, the period needs to be smaller than 200 nm.

4 Resonance Degradation at Small Periods

However, reducing the period also causes peak broadening and thus affects the color purity. For instance, when the period is smaller than 200 nm, the transmission hardly shows any resonant peak but shows an almost flat profile. In fact, the structure transits to a broadband wire grid polarizer.[3] The broadening in resonance is due to the reduced light confinement inside the slits. When a deep subwavelength metal slit illuminated by a TM wave with the electric field crossing the slit, polarization charges are accumulated at the corners and consequently distort the nearby field, making the slit opening a dipole.[15–17] At either the entrance or the exit side of the slit, the incident or the outgoing plane waves should couple into or out of the slit waveguide mode, leading to an impedance mismatch at the two interfaces. The impedance difference causes light reflection that is essential for the slit resonance. When slits are being arrayed, the interdistance plays an important role. For a 400-nm period, as shown in Fig. 4, the induced dipoles are separated from each other by a sufficient distance. Thus, the light field around each dipole is distorted, leading to an adequate impedance mismatch between the incident light and the slit waveguide mode. Consequently, light is well confined in the slits at a resonance, producing a distinct transmission peak.

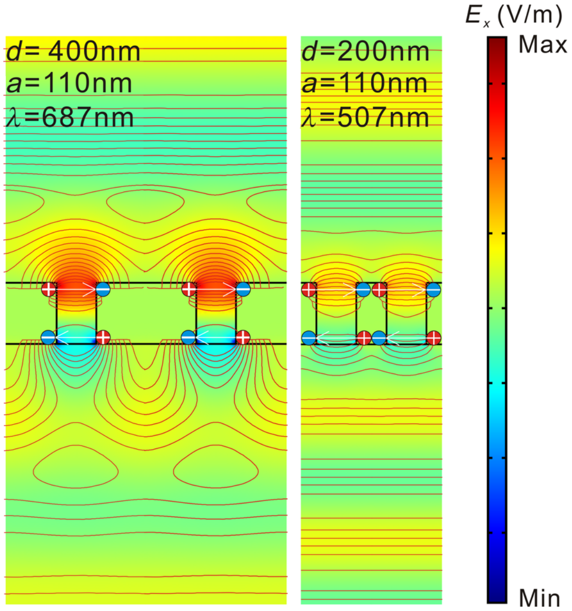

Fig. 4 Light field (E_x) distribution and electrical field lines in slit arrays with a 400-nm period and a 200-nm period under a normally incident plane wave with $E_0 = 3.92 \times 10^4$ V/m. The two structures are both on resonance at the wavelengths of 687 and 507 nm, respectively. Max: 2.44×10^5 V/m; Min: -2.90×10^5 V/m.

When the period decreases to 200 nm while the slit width remains the same, the induced dipoles adjacent to each other have an end-to-end configuration as shown in Fig. 4 so that the accumulated charges of opposite polarities tend to cancel out. Thus, the light field is only slightly distorted and the impedance mismatch to air is significantly reduced, leading to a much weaker resonance and a broadened transmission “peak.”

5 Maintaining a Sharp Resonance at Small Periods

5.1 *Decreasing the Slit Width*

Based on the above analysis, we anticipate that reducing the slit width can help to prevent resonance degradation, since the induced polarization charges are separated from their opposite neighbors and then survive cancellation, giving rise to a significant impedance mismatch by distorting the field at the slit opening [Fig. 5(a)].

By reducing the slit width to 50 nm at a 200-nm period, an angle-insensitive resonant transmission is achieved up to 60 deg with a bandwidth around 100 nm [Fig. 5(b)]. Actually, reducing the slit width not only makes up for the reduction in the interdistance, but also enhances the Q-factor of the intrinsic slit resonance due to the enlarged difference between the free-space wavelength and the slit width. As revealed by the spectra of the slit power enhancement factor

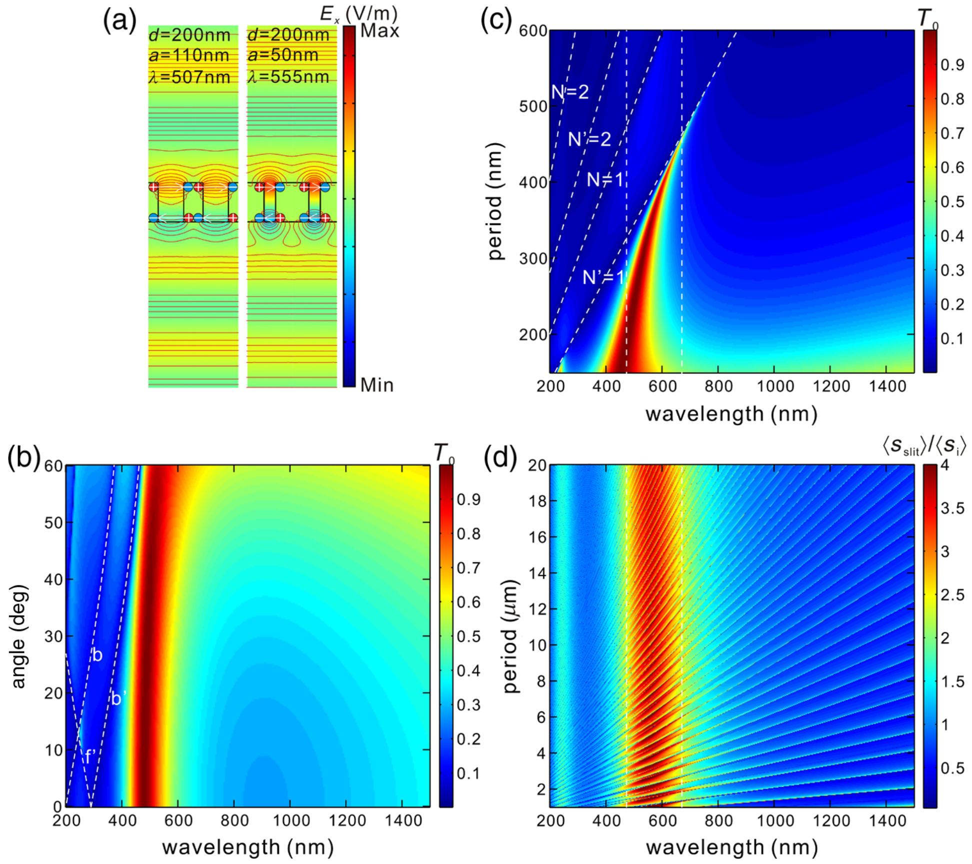

Fig. 5 (a) Light field (E_x) distribution and electrical field lines in two slit arrays with the same period 200 nm and different slit widths (110 and 50 nm) under a normally incident plane wave with $E_0 = 3.92 \times 10^4$ V/m. The two structures are both on resonance at the wavelengths of 507 and 555 nm, respectively. Max: 2.44×10^5 V/m; Min: -2.90×10^5 V/m. (b) and (c) Angle- and period-dependent zeroth-order transmission spectra of the structure with a 50-nm slit width. (d) Slit power enhancement factor versus wavelength and period. The thin dashed lines mark out the grating resonances. The area between the two vertical dashed lines marks out the slit resonance.

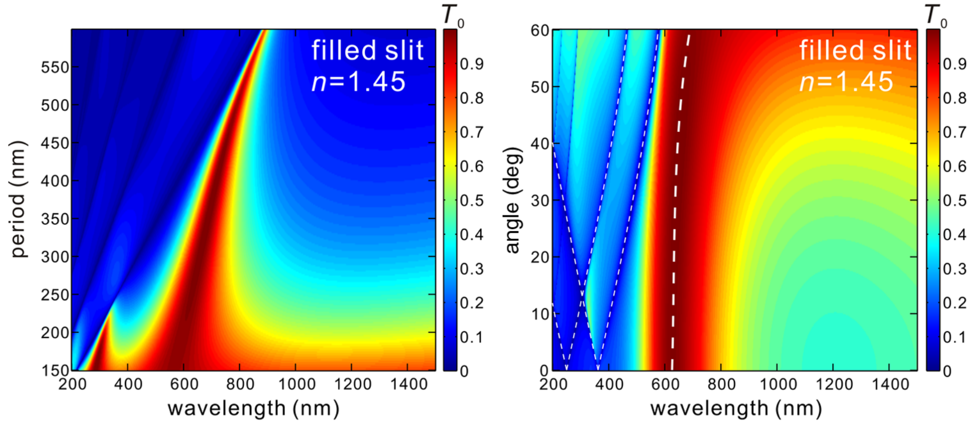

(a)

(b)

Fig. 6 Zeroth-order transmission spectra of arrayed slits filled by a medium with a refractive index of 1.45. Slit height is 170 nm; slit width is 110 nm. (a) Period-dependent zeroth-order normal incidence transmission spectra. (b) Angle-dependent zeroth-order transmission spectra at the period of 250 nm. The thin dashed lines mark out the Wood's anomalies. The thick dashed line marks out the transmission peak.

[Figs. 2(b) and 5(d)], the 110-nm-wide slit shows a resonance with a bandwidth of ∼450 nm, while the 50-nm-wide slit shows a resonance with a bandwidth of ∼200 nm.

5.2 *Filling the Slits with a High-Index Medium*

Another way to enhance light confinement inside the slits is to fill the slits with a high-index medium. Assuming that the slits are filled with a dielectric with an index of 1.45, the period-dependent zeroth-order transmission spectra are plotted in Fig. 6.

The slit height and width are still chosen to be 170 and 110 nm, respectively, so that the optical response can be compared with the air-slit case (Fig. 2). In general, the filled slits show a sharper slit resonance than the empty slits at the same period. The period of 250 nm, which gives a quite large angle-insensitive range (up to 50 deg), is chosen for the angle-dependent transmission spectrum plot [Fig. 6(b)]. Compared with air slits where the slit resonance is too weak to be identified from a high-transmission background, the dielectric-filled slits still exhibit a distinct resonance peak in transmission. Although the resonant wavelength of the filled slits is red shifted due to the increased optical path in a high-index material, the deviation can be compensated for by decreasing the slit height.

6 Slit Arrays Made of Real Metals

In order to show the validity of the above analysis in real metal cases, the transmission spectra for the slit array perforating an Al or Ag film are calculated by rigorous coupled-wave analysis and compared with the perfect electrical conductor (PEC) counterpart predicted by the analytical model. Except for the metal material, the geometry, the substrate, and the slit filler are the same for these three structures. The period is chosen to be 200 nm in order to have a large angle-insensitive range. To balance the peak broadening, the slit width is chosen to be 50 nm and the slits are filled by a medium with an index of 1.45. The slit height is chosen to be 120 nm to make the resonant transmission in the visible range. As shown in Fig. 7, both Al and Ag structures showing decent spectrum filtering behavior in transmission and the resonant peak at normal incidence is almost identical to that at a 30 deg oblique incidence, showing that the principles of achieving an angle-insensitive spectrum filter in the slit array structure are practical in real metal cases.

On the other hand, there are discrepancies between the real metal and the ideal metal cases. (1) The loss in real metal causes a lower peak transmission than the ideal metal case. (2) Both the Wood's anomalies and the slit resonance are red shifted in the spectrum of a real metal slit

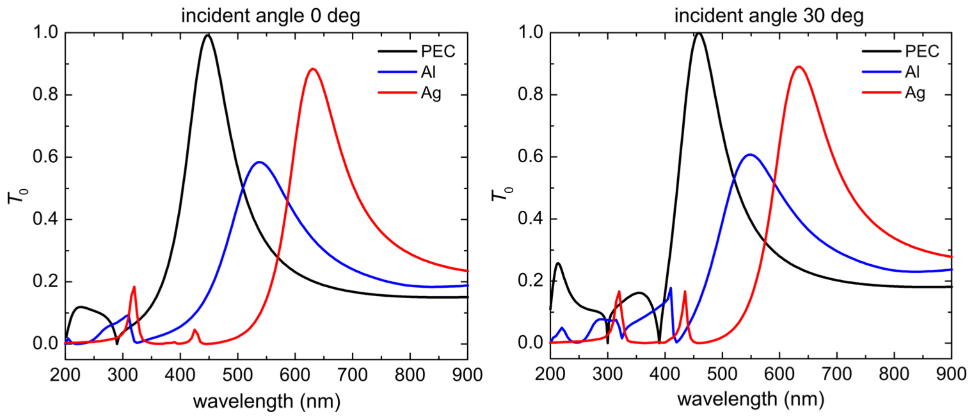

(a) (b)

Fig. 7 Zeroth-order transmission spectra of the slit array structure (period 200 nm, slit width 50 nm, and slit height 120 nm) made of perfect electrical conductor (PEC), Al, and Ag. The slits are filled by a medium with an index of 1.45. (a) Transmission at normal incidence. (b) Transmission at a 30-deg oblique incidence.

array with respect to that in the ideal metal case. This red shift is caused by SPP excitation. The Wood's anomaly in the ideal metal case is due to the wave being diffracted and propagated along the surface, while in real metal cases the Wood's anomaly is due to the SPP being excited at grating/air or grating/substrate interface [Fig. 8(a)]. The SPP wave is known to

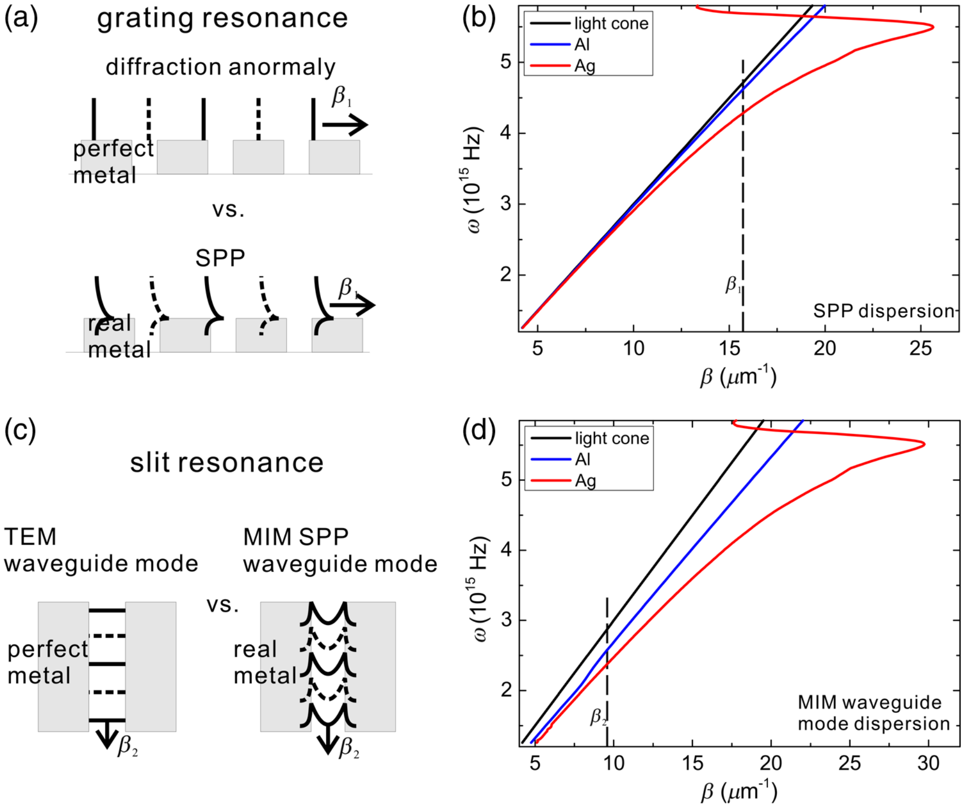

Fig. 8 Comparison between a slit array made of a perfect metal and that made of a real metal. (a) Sketch of surface light diffraction in a perfect metal slit array and the SPP wave in a real metal one. (b) Dispersion plots of light in free space (black curve), SPP wave at the Al/air interface (blue curve) and SPP wave at the Ag/air interface (green curve). (c) Sketch of the transverse electromagnetic (TEM) waveguide mode in a perfect metal slit and the MIM SPP mode in a real metal slit. (d) Dispersion plots of TEM waveguide mode, Al/air/Al SPP mode, and Ag/air/Ag SPP mode in a slit of 110-nm wide.

have a higher momentum due to its special dispersion [Fig. 8(b)], therefore, it occurs at a longer wavelength.

With a propagation constant $\beta_1 = 2\pi/d$ given by the grating, the surface wave in the ideal metal case occurs at a frequency of $\omega = (2\pi c/d)$, where c is the light speed; the SPP in a real metal case occurs at $\omega = (2\pi c/d)\sqrt{(\varepsilon_\mathrm{m} + \varepsilon_\mathrm{i})/\varepsilon_\mathrm{m}\varepsilon_\mathrm{i}}$, where ε_m is the permittivity of the metal and ε_i is that of the dielectric. Similarly, the waveguide mode in a slit with ideal metal walls is a transverse electro-magnetic (TEM) mode with free space momentum; while that in the real metal case is an MIM SPP mode [Fig. 8(c)] with higher momentum and thus causes a red shift of the slit resonance. The MIM SPP mode follows the dispersion

$$\tan h[\frac{a}{2}\sqrt{\beta^2 - \varepsilon_\mathrm{i}(\omega/c)^2}] = -\frac{\varepsilon_\mathrm{i}\sqrt{\beta^2 - \varepsilon_\mathrm{m}(\omega/c)^2}}{\varepsilon_\mathrm{m}\sqrt{\beta^2 - \varepsilon_\mathrm{i}(\omega/c)^2}}$$

and is plotted in Fig. 8(d). Since Ag has a lower plasma frequency (13.70×10^{15} Hz, i.e., wavelength ~138 nm) than Al (22.43×10^{15} Hz, i.e., wavelength ~84 nm), the dispersion of Ag SPP deviates more from the light cone than that of Al SPP [Figs. 8(b) and 8(d)], therefore, the Wood's anomaly and the slit resonance are more red-shifted.

Concerning the Wood's anomalies as well as the slit resonance either in a real metal case or in the ideal metal case, the principle is similar. The former is based on grating diffraction and the latter is based on Fabry-Perot resonance, no matter whether the mediating wave is an SPP or not. Therefore, the guidelines of creating an angle-insensitive spectrum filter with a narrow transmission peak, based on our theoretical model, also work for the real metal cases.

7 Conclusion

In summary, to address angle dependence of the spectrum filter based on the slit nanoresonator array structure, the coupling between the slit resonance and the Wood's anomaly should be removed. Although a reduction in period can achieve this purpose, the broadening of the resonance peak due to the reduced light confinement inside the slits hinders practical usage. However, by reducing the slit width or by filling the slit with a high-index medium, an adequate impedance difference and a good light confinement can be maintained, and as a result, relevant angle-insensitive spectrum filtering can be achieved.

Acknowledgments

The authors would like to acknowledge the National Science Foundation (ECCS 1202046) for the support of this work.

References

1. A. F. Kaplan, T. Xu, and L. J. Guo, "High efficiency resonance-based spectrum filters with tunable transmission bandwidth fabricated using nanoimprint lithography," *Appl. Phys. Lett.* **99**, 143111 (2011).
2. Y. R. Wu et al., "Angle-insensitive structural colours based on metallic nanocavities and coloured pixels beyond the diffraction limit," *Sci. Rep.* **3**, 1194 (2013).
3. J. Zhou and L. J. Guo, "Transition from a spectrum filter to a polarizer in a metallic nanoslit array," *Sci. Rep.* **4**, 3614 (2014).
4. H. J. Park et al., "Photonic color filters integrated with organic solar cells for energy harvesting," *ACS Nano* **5**, 7055–7060 (2011).
5. K. Lee et al., "Enhancing surface plasmon detection using template-stripped gold nanoslit arrays on plastic films," *ACS Nano* **6**, 2931–2939 (2012).
6. J. Yao et al., "Soft embossing of nanoscale optical and plasmonic structures in glass," *ACS Nano* **5**, 5763–5774 (2011).
7. M. A. Schmidt et al., "Hybrid nanoparticle-microcavity-based plasmonic nanosensors with improved detection resolution and extended remote-sensing ability," *Nat. Commun.* **3**, 1108 (2012).

8. E. Cho et al., "Two-dimensional photonic crystal color filter development," *Opt. Express* **17**, 8621–8629 (2009).
9. S. Collin et al., "Horizontal and vertical surface resonances in transmission metallic gratings," *J. Opt. A-Pure Appl. Opt.* **4**, S154–S160 (2002).
10. F. Marquier et al., "Resonant transmission through a metallic film due to coupled modes," *Opt. Express* **13**, 70–76 (2005).
11. P. Catrysse et al., "Guided modes supported by plasmonic films with a periodic arrangement of subwavelength slits," *Appl. Phys. Lett.* **88**, 031101 (2006).
12. T. Kim et al., "Control of optical transmission through metals perforated with subwavelength hole arrays," *Opt. Lett.* **24**, 256–258 (1999).
13. F. J. Garcia-Vidal et al., "Light passing through subwavelength apertures," *Rev. Mod. Phys.* **82**, 729–787 (2010).
14. D. Pacifici et al., "Quantitative determination of optical transmission through subwavelength slit arrays in Ag films: role of surface wave interference and local coupling between adjacent slits," *Phys. Rev. B* **77**, 115411 (2008).
15. P. Lalanne and J. P. Hugonin, "Interaction between optical nano-objects at metallo-dielectric interfaces," *Nat. Phys.* **2**, 551–556 (2006).
16. P. Lalanne et al., "A microscopic view of the electromagnetic properties of sub-lambda metallic surfaces," *Surf. Sci. Rep.* **64**, 453–469 (2009).
17. A. Y. Nikitin, F. J. Garcia-Vidal, and L. Martin-Moreno, "Surface electromagnetic field radiated by a subwavelength hole in a metal film," *Phys. Rev. Lett.* **105**, 073902 (2010).

Jing Zhou is a postdoctoral research fellow at the University of Michigan. He received his BS degree and a PhD degree in optics from Fudan University, Shanghai, China, in 2006 and 2011, respectively. His current research interests include nano- and micro-photonics, metamaterials, and nanofabrication.

L. Jay Guo is a professor of electrical engineering, applied physics, macromolecular science, and mechanical engineering at the University of Michigan. He received his PhD degree from the University of Minnesota. He has over 220 publications, which have been cited more than 18,000 times. His current research interests include nano- and micro-photonics, organic electronics and photonics, nanofabrication, and ultrasonics.